Solute rich cluster formation and Cr precipitation in irradiated Fe-Cr-(Ni,Si,P) alloys: Ion versus neutron irradiation

C. Pareige[a*], A. Etienne[a], P-M. Gueye[a], A. Medvedev[a], C. Kaden[b], M.J. Konstantinovic[c], L. Malerba[d]

[a] *Normandie Univ, UNIROUEN, INSA Rouen, CNRS, Groupe de Physique des Matériaux, 76000 Rouen, France*
[b] *Institute of Resource Ecology, Helmholtz-Zentrum Dresden - Rossendorf, Dresden, 01328, Germany*
[c] *Studiecentrum voor Kernenergie / Centre d'Étude de l'Énergie Nucléaire (SCKCEN), Mol (Belgium)*
[d] *Centro de Investigaciones Energéticas, Medioambientales y Tecnológicas (CIEMAT), Madrid, Spain*

Abstract

Ion irradiation is a powerful and affordable tool to rapidly test a wide range of irradiation conditions and make the link with the corresponding microstructural evolution. However, several issues of transferability of results from ion to neutron irradiation have been evidenced. This paper presents an atom probe investigation of the microstructural evolution of FeCr-NiSiP alloys with different contents of Cr and minor solutes under both ion and neutron irradiation at 300 °C. Minor solutes and Cr are known to form solute rich clusters (SRCs) and α' clusters in ferritic and martensitic FeCr alloys, which are one of the causes of hardening. The objective of this work is to highlight the differences and the commonalities between ion and neutron irradiations in these alloys. The use of two ion beam energies (8 MeV and 5 MeV) revealed that this parameter has an impact on the formation of SRCs. The SRCs present similar characteristics after 8 MeV Fe ion irradiation and neutron irradiation, despite the different dose rate, when Ni, Si and P are present. It is not the case for 5 MeV Fe ions, for which the SRCs were less developed. Influence of the concentration of minor elements has been evidenced, as well. The presence of Ni, Si and P has been shown to impact both the number density and the size of SRCs in Fe9Cr-NiSiP alloys and the onset of α' formation.

1. Introduction

The development and qualification of high-chromium ferritic-martensitic (F-M) steels for GEN IV or fusion applications require a profound understanding of the mechanisms of neutron damage. Ion irradiation is a powerful and affordable tool to rapidly test a wide range of irradiation conditions and make the link with the corresponding microstructural evolution. However, several issues of transferability of results from ion to neutron irradiation have been evidenced [1–8]. Their origin is connected with the charged nature of ions and the possibilities offered by ion irradiation devices. The dose rate is lower in neutron ($<10^{-7}$ dpa/s) as compared to ion ($> 10^{-5}$ dpa/s) irradiation, in addition ions only penetrate a thin layer of material and produce non-uniform damage within the affected thickness [4,5,7,9]. Besides, self-ion irradiation introduces additional atoms, also according to a non-uniform distribution (injected interstitials) [3]. The effect of increasing dpa-rate can be partly compensated by irradiation variable shifts, e.g. in temperature or dpa (displacement per atoms). However, no single temperature shift is able to guarantee ion/neutron equivalence for the whole variety of irradiation-induced/enhanced microstructural features [5,10–13], at the same dpa level and such a temperature shift has not been clearly evidenced for ferritic alloys.
In ferritic and martensitic alloys, solute atoms such as Si, P, Cu, Ni, Cr, Mn are known to form radiation-induced clusters or radiation-enhanced precipitates [14–19]. In Fe-Cr alloys containing Ni, Si and P at minor solute level, three types of nanofeatures have been shown to be responsible for radiation-induced hardening, namely: dislocation loops and solute rich clusters (SRCs) containing Ni, Si, P and Cr for any Cr content, as well as Cr-rich clusters (α' clusters) in Cr supersaturated alloys [15,17,20–23]. SRCs have been shown to play a major role on irradiation hardening [20]. Konstantinovic et al. [24]

observed that the ferritic alloys containing more Ni, Si and P hardens more than the martensitic one. Evolution of the matrix damage appears more sensitive to the Ni, Si and P content than to the initial microstructure (ferritic vs martensitic) [25] Whereas α' formation is enhanced by radiation [15–17], SRCs are radiation induced clusters [14,15,26–28]. Under ion irradiation, the formation of α' clusters has been shown to be very sensitive to injected interstitials [3] and to high dose rate [4]: both limit the formation of these clusters. Thus irradiation induces effects on α' precipitation, as well. For a full understanding of the effect of the irradiation conditions on SRC formation and evolution, therefore, it is necessary to explore the effect of different variables on the observed population of solute clusters and precipitates. For this purposethree alloys containing 9%Cr and various minor solute levels, mainly Ni, Si and P, have been neutron and ion irradiated under similar conditions. In this work, we report the result of atom probe tomography (APT) on these materials, in order to evaluate the difference in SRCs and Cr-rich α' clusters evolution, depending on the type of irradiation.

2. Materials and experiments

2.1. Materials

The composition and the initial microstructure (ferritic or martensitic) of the three Fe-9%Cr model alloys with three total minor solute levels (0.02at.%, 0.27at.% and 0.56 at.%) that were investigated are provided in Table 1. The ferritic model alloys were cast by OCAS (Belgium) in an induction vacuum furnace. The pure Fe source contained only 50 ppm Co and 70 ppm Ni, while all other elements were below 10 ppm. No contamination due to the addition of the electrolytically refined Cr source is expected. The final composition was determined by solid sampling optical emission spectroscopy (SS-OES), except for Ni, Si and Al which were quantified using inductively coupled plasma OES (ICP-OES). All elements not given in the table were below the SS-OES detection limits, except for the S content which lies between 10 and 15 ppm for all casts. From each ingot, a piece of 50 mm × 125 mm × 250 mm was cut from the bottom and heat treated in a pre-heated furnace at 1200°C for 1 h 30 min. Subsequently, the material was hot rolled and finally air-cooled down to room temperature resulting in a fully ferritic microstructure. The grain size are the following: 25 µm for Fe9Cr_X0, 27 µm for Fe9CrNiSiP with a dislocation density of 4.2×10^{13} m^{-3} in Fe9Cr_X0 [29].
The martensitic alloy, Fe9Cr-NiSiP_X1, was fabricated at the University of Ghent (Belgium) by furnace melting Fe and Cr of industrial purity. The cast ingot was cold worked under protective atmosphere to 9 mm thick plates and annealed for 3 hours at 1320 K in high vacuum for austenitization and stabilization, followed by air cooling. Subsequently, the material was tempered at 1000 K for 4 hours. The heat treatment resulted in a tempered martensite microstructure with a minor amount of ferrite. The chemical composition was measured using ICP mass spectroscopy and combustion technique at OCAS. The grains are similar to martensitic laths but the laths consist of ferrite grains with a density of dislocations 6.3×10^{13} cm^{-2} [22,30] and a broad distribution of grain size of the order of 1 µm.
APT characterisation and statistical tests performed on the unirradiated alloys showed that the alloys are fully random [15,28,29,31].

Table 1: Composition measured by SS-OES and ICP-OES and microstructure of the selected FeCr(NiSiP) alloys (in at.%).

Name*	Code	Fe	Cr at.%	Ni at.%	Si at.%	P at.%	Al at.%	(Ni+Si+P) at.%	Micro-Structure
Fe9Cr_X0	G385	Bal.	9.7	0.009	0.008	0.005	0.055	0.02	Ferritic
Fe9Cr-NiSiP_X1	L252	Bal.	8.9	0.066	0.18	0.021	0.014	0.27	Martensitic
Fe9Cr-NiSiP_X2	G389	Bal.	9.7	0.087	0.42	0.057	0.057	0.56	Ferritic

* X0: minor solutes at level 0, X1: minor solutes at level 1, X2: minor solutes at level 2

2.2. Irradiation conditions

Samples of the FeCr alloys were neutron irradiated in the BR2 material testing reactor of SCK-CEN at 290°C. They were exposed to a neutron flux of about 1.5 10^{13} $cm^{-2}s^{-1}$ for two 3-weeks reactor cycles and received a total fluence of 1.1 10^{20} cm^{-2} (E > 1 MeV). According to dosimetry, the neutron fluence and flux received correspond to a displacement damage of 0.11 dpa and a displacement rate of 2.2 10^{-8} dpa/s, respectively. More details are available in [24].

Samples of the same materials intended for ion irradiation were cut to the dimensions of 8-10 x 10 x 1 mm^3 and mirror polished using mechanical grinding and polishing in several steps, down to diamond suspension of 1 µm particle size. The remaining surface damage introduced by mechanical polishing was removed by low-temperature (~ 0°C) electropolishing using a solution of 98% of ethylene glycol monobutyl ether and 2% of perchloric acid [32]. Unirradiated samples that served as reference samples were prepared using the same preparation method.

Ion irradiations were performed at a temperature of 300°C with self-ions (Fe^{3+}) of an energy of 8 MeV using a 3MV-Tandetron accelerator at the Ion Beam Center of HZDR, Dresden, Germany. This choice of the energy is expected to provide a sufficiently large midrange region far from both the near surface region and the implantation peak that must be avoided to prevent artefacts [3,7]. A reference depth of 500 nm was chosen as target for the microstructural analysis. The irradiation was designed in such a way that the nominal displacement damage of 0.1 dpa, as for neutron irradiation, was reached at this depth. The damage and implantation profiles are presented in *Figure 1*. They were calculated using SRIM (Stopping and Range of Ions in Matter) [33,34] with the ‘‘Quick Kinchin-Pease calculation” mode using 40 eV as the displacement threshold for Fe [35] and following the recommendations of Stoller *et al.* [36]. In order to guarantee a homogeneous lateral exposure over the whole set of samples, the focussed ion beam was scanned over the area of the samples during the irradiation. The scanning frequencies were 1 041 Hz and 1 015 Hz in horizontal and vertical directions, respectively. Scanning of the beam has been shown to impact the swelling kinetics [37]. But rastering is expected to not impact segregation and precipitation behaviour. The ion flux was measured continuously by means of Faraday cups (measurement of current) and integrated to obtain the ion fluence. The irradiation temperature was maintained by fixing the samples on a heating target. The temperature control was based on a thermocouple placed on the backside of one sample. Temperature for ion irradiation has been chosen similar to the one used for neutron irradiations for two reasons. The first reason concerns the study of α' precipitation which is an enhanced mechanism. The goal here is to investigate the influence of the nature of the irradiation on the kinetics keeping the driving force of α' precipitation constant. The second reason concerns the formation of the SRCs. APT results obtained in Fe-Cr(NiSiP) alloys irradiated at 0.5 dpa at 300 °C with neutrons and with Fe ions of 5 MeV within the GETMAT project [14] did not reveal significant differences. Moreover, in ferritic alloys, a systematic temperature shift has not been clearly evidenced in the literature. The ion irradiation parameters in terms of ion fluence and flux, as well as the corresponding displacement damage and damage rate at 500 nm depth, are the following: fluence equal to 4.16x10^{14} cm^{-2} (0.1 dpa), flux equal to 7.6x10^{10} $cm^{-2}s^{-1}$ (1.8x10^{-5} dpa s^{-1}).

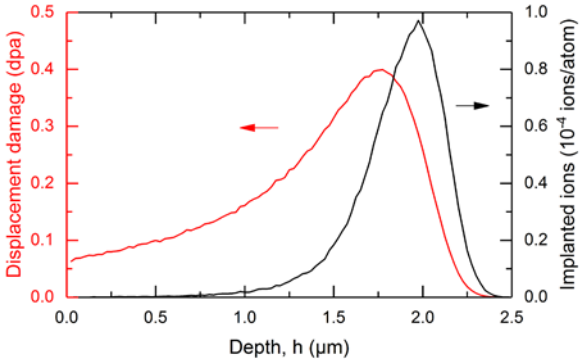

Figure 1: Displacement damage and injected Fe concentration profiles for an Fe ion energy of 8 MeV and a target displacement damage level of 0.1 dpa at 500 nm.

2.3. Atom probe tomography (APT)

The neutron irradiated APT samples were prepared using the classical electropolishing method [38]. In case of the ion irradiated alloys, the APT samples were lifted-out and annularly milled using a Scanning Electron Microscope – Focus Ion Beam (SEM-FIB ZEISS Crossbeam XB540). Annular milling was performed to reach a depth of 400-500 nm from the surface, in order to analyse the region corresponding to a displacement damage of 0.1 dpa. The final milling was undertaken with a Ga beam energy of 2 kV, which limits implantation of Ga ions in the material. At least three APT samples were analysed for each condition. The APT volumes were extracted from at least two or three different places over the samples, guaranteeing analysis of different grains.

The samples were examined using LEAP 4000X HR Atom Probes from AMETEK-CAMECA, which are equipped with a Delay Line Detector (DLD) [39] of 36% efficiency. The LEAP HR are equipped with a reflectron, which provides a high mass resolution and improves the accuracy of composition measurements. The samples were analysed at 55 K, as this temperature avoids preferential evaporation of Cr atoms. The specimens were electrically pulsed with a pulse fraction of 20% of DC voltage at a pulse repetition rate of 200 kHz. The detection rate was set up between 0.1% and 0.35% in order to obtain a specimen flux of about 0.25-0.35 ions/nm^2/s. The APT volumes were reconstructed using IVAS 3.6.8 (CAMECA software). The compression factor ξ was set to 1.65, which corresponds to the value obtained from the crystallographic angles between poles observed on the desorption maps in these alloys. The field factor k was derived from the expected interplanar distance at the poles. k ranged between 3.7 and 4.9 depending on the nature of the tip support used (i.e. electropolished tip or tip on micro-coupon) and depending on each sample.

The APT data were treated using the 3D Software developed by the GPM, University of Rouen Normandie, France. The behaviour of the different species under irradiation was investigated using both statistical tools and iso-concentration filtering, the latter to isolate clusters or precipitates. The iso-concentration method (ICM) [38,40,41] that was used for the identification of clusters or precipitates in the irradiated samples is based on three parameters: a concentration threshold (C_{th}) criterion, a minimum number of relevant atoms (N_{min}) that are detected in the clusters and a distance d corresponding to the distance below which two atoms belong to the same cluster (d = 0.5 nm). The selection of the parameters C_{th} and N_{min} is made in such a way that ghost clusters are avoided in a random solid solution of the same composition. C_{th} ensures that less than 0.01% of the filtered atoms in the random solution would have this concentration [41] (in ref [41], a value of 0.1% is given but it is a misprint). N_{min} is chosen in order to identify zero clusters in the random solution for the selected C_{th} value. These parameters were estimated for each APT volume considering a randomized solid solution

of the same composition. The variation of the parameters C_{th} and N_{min}, which are required to reliably detect irradiation-induced clusters, is linked to the variation of the nominal concentration of the considered species from one tip to another. Depending on the investigated alloy, the ICM was applied either based on the P concentration or based on Ni+P+Si concentration. The important point is to ensure that the choice made allows the correct identification (in size and shape) of all the clusters visible on the 3D images.

The number density (N_V) of the identified clusters corresponds to the ratio of the number of observed clusters to the overall analysed volume. After application of the ICM, clusters are often found to be surrounded by matrix atoms, which are erroneously associated with the clusters. These shells are systematically removed using an erosion method before measuring the size [38]. The radius of each cluster was calculated considering them as spherical:

$$R = \sqrt[3]{\frac{3nV_{at}}{4\pi Q}} \qquad (1)$$

with n the number of atoms into the cluster, V_{at} the Fe atomic volume ($a_0^3/2$ with a_0 the lattice parameter) and Q the detector efficiency. The cluster's composition was measured in the core (on the plateau) of the clusters using erosion concentration profiles [38]. The concentration values are thus not affected by the interface. It is worth noting that the particle composition must not be measured considering the same atoms that were used to calculate the size, to avoid including the interface atoms in the measurement. If this was done the matter conservation law would be violated. Radius, number density and composition values were averaged over all the APT volumes for each condition. At least three APT samples from at least two different grains have been investigated for each condition.

3. Results

3.1. Solute rich clusters

Figure 2 compares the P distribution after ion and neutron irradiations. In both cases, clusters are clearly visible: even in Fe9Cr_X0, where the P concentration is only 0.005 at.%. In this material, the P cluster density is lower under ion irradiation. However, for Fe9Cr-NiSiP_X1 and Fe9Cr-NiSiP_X2, 3D images show very similar microstructure in both ion and neutron irradiated specimens.

The characteristics of the solute rich clusters are summarized in Table 2. Composition measurements carried out in the core of the clusters show that these are enriched in P, Ni, Si and Cr except for Fe9Cr_X0 where only an enrichment in P and Cr is observed. The radius distributions are provided in Figure 3. In good agreement with 3D images, the SRC composition, number density in Fe9Cr-NiSiP_X1 and Fe9Cr-NiSiP_X2, are very similar under neutron and ion irradiation.
The average size is slightly larger under neutron irradiation however because of the uncertainties it is difficult to conclude from this data alone. Comparison of radius distributions is necessary. The radius distributions are presented in Figure 3a and b. A significant shift is observed and confirm the trend: the distributions are shifted toward larger values after neutron irradiation.
Comparison of radius distributions between Fe9Cr-NiSiP_X1 (martensitic) and Fe9Cr-NiSiP_X2 (fully ferritic) in Figure 3c and d, reveals a slightly higher proportion of smaller SRCs when the NiSiP content is higher whatever the nature of the irradiation. The number density increases and the size decreases with increase in minor solute content for alloys containing Ni, Si and P.
In Fe9Cr_X0, SRC are less enriched in Cr and P after ion irradiation and their number density is 3.5 times lower.

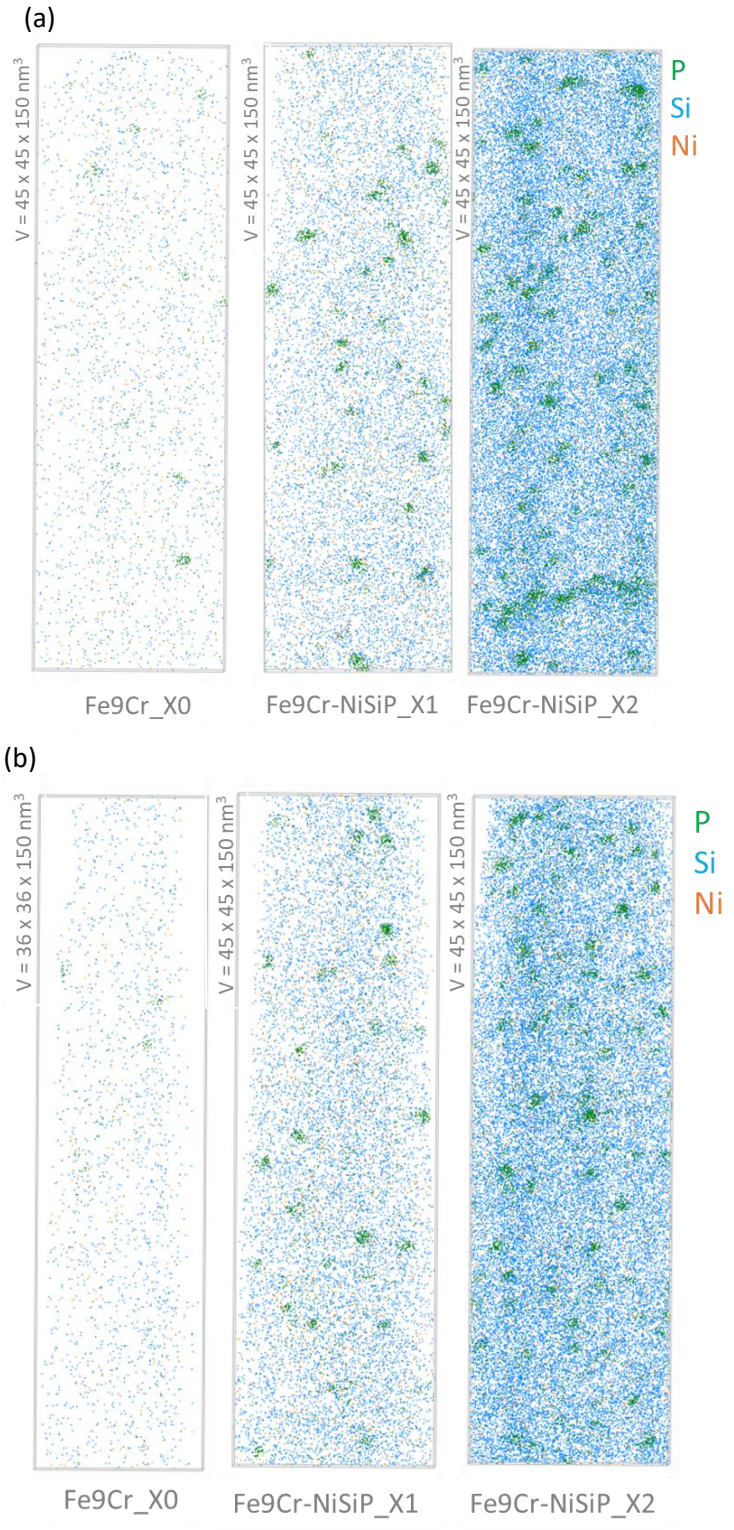

Figure 2: Distribution of P atoms in the three alloys (a) after neutron irradiation and (b) ion irradiation up to 0.1 dpa. No data filtering has been applied.

Table 2 : SRC composition (in at.%), number density and radius after neutron and ion irradiations at 0.1 dpa, 300 °C.

	Fe9Cr_X0		Fe9Cr-NiSiP_X1		Fe9Cr-NiSiP_X2	
	Neutrons	*Ions*	Neutrons	Ions	*Neutrons*	*Ions*
Fe (at.%)	*Bal.*	*Bal.*	*Bal.*	*Bal.*	*Bal.*	*Bal.*
Cr (at.%)	19.9 ± 3.3	17.8 ± 2.4	17.7 ± 0.6	16.4 ± 1.5	17.9 ± 2.5	14.8 ± 0.7
Ni (at.%)	-	-	2.7 ± 0.4	2.0 ± 0.3	1.9 ± 0.4	1.3 ± 0.5
Si (at.%)	-	-	1.4 ± 0.2	1.0 ± 0.2	1.8 ± 0.5	1.7 ± 0.9
P (at.%)	8.2 ± 0.9	4.4 ± 1.3	6.4 ± 1.2	6.2 ± 0.8	7.1 ± 1.6	7.0 ± 0.5
Nv (10^{23} m^{-3})	0.34 ± 0.1	0.09 ± 0.04	1.4 ± 0.2	1.3 ± 0.2	3.3 ± 0.3	3.1 ± 0.4
R (nm)	1.1 ± 0.7	1.2 ± 0.2	1.8 ± 0.4	1.7 ± 0.4	1.7 ± 0.4	1.5 ± 0.4

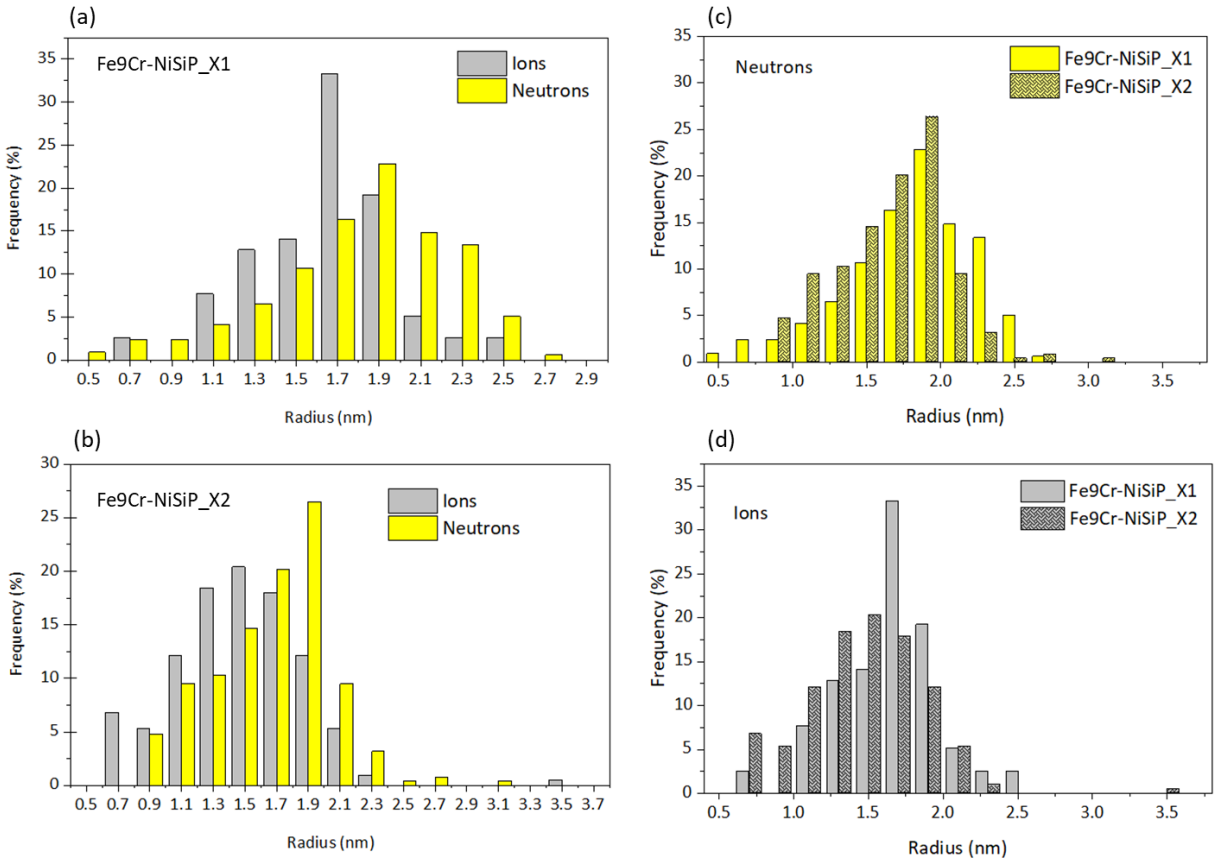

Figure 3: Radius distributions of SRCs in Fe9Cr-NiSiP_X1 and Fe9Cr-NiSiP_X2 after neutron (yellow) and ion (grey) irradiations at 0.1 dpa at 300 °C. (a) and (b): ion versus neutron for each alloy. (c) and (d) Fe9Cr-NiSiP_X1 versus Fe9Cr-NiSiP_X2 for each irradiation type.

3.2. Cr rich particles

Figure 4 presents the 3D distribution of Cr and P atoms for the three alloys after neutron (a) and ion (b) irradiation, respectively. For Fe9Cr-NiSiP_X1 and Fe9Cr-NiSiP_X2 under both neutron and ion irradiation: the Cr rich regions that are visible on the images correspond to the SRCs which have been shown to be enriched in Cr (Table 2). On the images, it is indeed possible to see that the Cr-rich regions visible on the images are associated with P rich regions for both irradiation conditions. Some of these SRCs are highlighted with arrows. Except these zones, no Cr rich clusters which could be associated with α' clusters are present.

For Fe9Cr_X0: surprisingly, the Fe9Cr_X0 behaves differently under neutron irradiation. For this alloy, the major part of the Cr rich clusters appearing on the images are not associated with the P clusters. These Cr rich clusters are therefore α' clusters. Their average radius is (1.1 ± 0.2) nm, their number density is 2×10^{23} m^{-3} and the Cr content equals (45 ± 3) at.%. Figure 4(a) presents a concentration profile drawn through one α'cluster. The fact that α' clusters are not observed in Fe9Cr-NiSiP_X1 and _X2 alloys (rich in Ni, Si and P) but are observed in the Fe9Cr_X0 alloy, suggests that the presence of minor solutes with significant binding to vacancies [26] impacts the kinetics of formation of the α' particles at early stages. Under ion irradiation, no α' cluster is visible on the images and no α' cluster has been detected using concentration filtering.

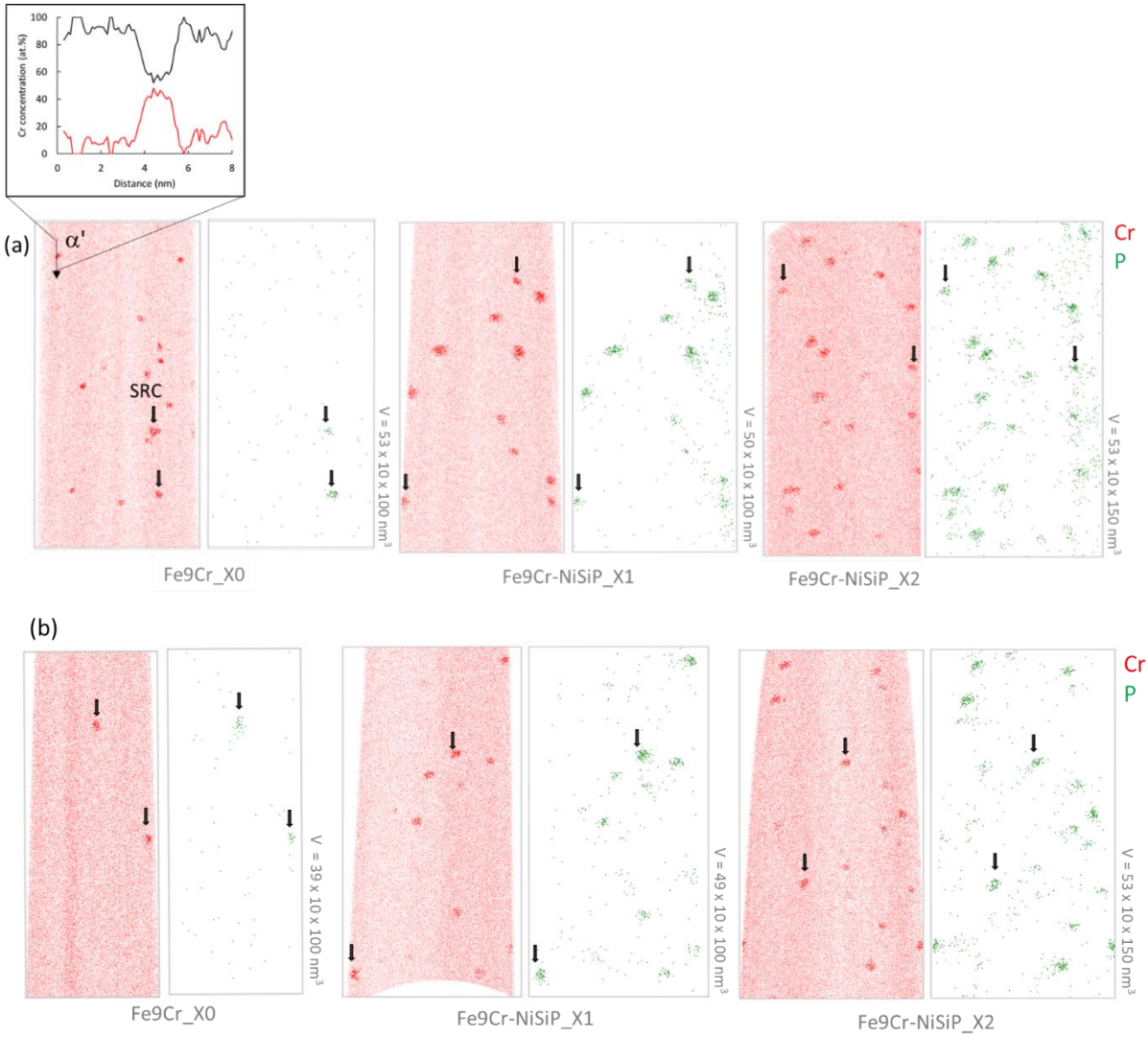

Figure 4: Distribution of Cr and P atoms in the three alloys after neutron irradiation (a) and ion irradiation (b) at 0.1 dpa. A concentration profile drawn through a α' cluster is presented. Arrows higlight some of the SRCs in Cr and P maps. A concentration threshold X_{Cr}>16at.% was used to highligt Cr rich regions.

4. Discussion

SRCs are equally observed under neutron and ion irradiation in all the alloys that have been studied in this work. Even in Fe9Cr_X0, with only 0.005 at.% P, PCr rich clusters are observed. P is the minor solute with the highest concentration in SRCs, whereas its nominal concentration is the lowest. The enrichment factor (X_P^{SRC}/X_0) is ~125 in Fe9-NiSiP_X2 alloys, ~300 in Fe9Cr-NiSiP_X1 and ~1600 in Fe9Cr_X0. This confirms the strong segregation tendency of P, as already mentioned in previous experimental and numerical works [40,42–45]. P atoms are the fastest diffusers [46,47] as P creates very stable complexes both with self-interstitials (mixed dumbbells, binding energy ~1 eV) and vacancies (P-vacancy pairs, binding energy ~0.4 eV) [46,47]. Moreover, P mixed dumbbells are trapped by other P atoms in the matrix [46,47]. These immobilized dumbbells could be stable nuclei of dislocation loops and act as point defect sinks that are further enriched by dragging of solute atoms (P, Ni, Si and Cr). Experimental results of Hardouin-Duparc [45] highlighted the link between P and the increase in the number density of dislocation loops in electron irradiated Fe–P. In good agreement with this scenario, recent APT results of Gueye et al. [28] showed that SRCs are more enriched in P at low dose than at higher dose and that at higher dose, small decorated dislocation loops with the same composition than SRCs appear. Recent OKMC (Object Kinetic Monte Carlo) simulations [26] clearly highlighted the dominant role of the immobilized point defect clusters on the nucleation process of SRCs and confirmed the radiation induced nature of SRCs. Higher NiSiP concentrations lead to an increase in SRC number density, with corresponding decrease in size of SRCs (Table 2), because a larger number of nuclei (immobilized point-defect clusters) forms, on which the solutes redistribute. The same observation in terms of number density and size evolution for dislocation loops in these alloys which were neutron irradiated in the same conditions, has been reported by Dubinko et al. [25]: a decrease of the size of dislocation loops accompanied by an increase in number density with the increase in Ni, Si and P content. APT, TEM (Transmission Electron Microscopy) and OKMC results are thus very consistent with the hypothesis that the invisible small dislocation loops (small interstitial clusters) correspond to the SRCs observed in APT volumes and the growth of SRCs leads to the formation of decorated dislocation loops.

Under neutron irradiation, in the Fe9Cr set of alloys, well defined Cr rich clusters are only observed in the Fe-9Cr_X0 alloy. In contrast, no α' precipitates were observed in the Fe9Cr-NiSiP alloys. The presence of α' clusters in Fe9Cr-NiSiP_X1 has been reported, but at higher dose, namely 0.5 dpa [15]. The number density was $(2.1 \pm 0.2)\times10^{23}$ m^{-3} and the average radius (1.1 ± 0.2) nm, very similar values to those measured in Fe-9Cr_X0 at 0.1 dpa. The presence of NiSiP seems therefore to induce a delay in the onset of α' clusters formation in Fe-9Cr alloys for which the driving force for α' precipitation is low. These results are consistent with PAS and SANS measurements [25]. This might originate from the competition between solute species that are dragged by point-defects. Specifically, due to the stronger interaction of vacancies with, in order P (~ 0.4 eV), Si (~ 0.3 eV) and Ni (~ 0.2 eV) than with Cr (<0.1 eV) [43], these defects will preferably be bound to the minor solutes than to Cr, thereby delaying the diffusion of Cr to form precipitates. Another reason is the competition of the formation of SRCs and α' particles which are both enriched in Cr. It is expected that this competition would have a greater effect in the case of alloys that are close to the solubility limit. Simulations or complementary experiments should be performed to clarify this point.

α' clusters have been observed in Fe9Cr_X0 under neutron irradiation but not under ion irradiation. This is very likely the result of the higher dose rate of ion irradiation, which increases the dissolution by ballistic effect [4,48]. . If we consider SRCs, there is no significant quantitative difference between 8 MeV Fe ion- and neutron-irradiated in Fe9Cr-NiSiP_X1 and Fe9Cr-NiSiP_X2 alloys: number density and composition of SRCs are similar. The only difference concerns a slight shift of the size distribution towards higher values in case of neutron irradiation. Thus, there seems to be only a slight dose-rate effect on the formation of SRCs in Fe9Cr-NiSiP alloys with 8 MeV ions. This reveals that dose-rate

effects are more visible in some microstructural features than in others. Namely, the characteristics of α' clusters are more sensitive to dose-rate than those of NiSiP clusters. The sensitivity of Cr-rich clusters to dose-rate has been ascribed to ballistic dissolution [4,48]. As the formation mechanism is different, perhaps the dpa-rate above which ballistic dissolution plays a role is different/higher for SRCs. Dedicated modelling should be able to help to answer this question. In contrast, in Fe9Cr_X0, the number density and the P concentration of PCr clusters is lower after 8 MeV ion-irradiation than after neutron-irradiation. In this alloy, therefore, a dose-rate effect is observed. The dose-rate effects are more or less visible depending on the content of minor element. These results show that minor elements, which present strong interactions with point defects, impact significantly the behavior of these alloys under irradiation.

5. Conclusion

Three alloys with 9%Cr and various minor solute levels of Ni, Si and P, have been ion and neutron irradiated at 300 °C up to 0.1 dpa and have been characterized by APT. This work has shown that:

- SRCs number density increases and size decreases when the Ni-Si-P content increase. Comparison with TEM and OKMC data [25] confirms that SRCs observed in APT volumes are very likely TEM invisible small dislocation loops.
- Similar microstructure after both 8 MeV ion irradiation and neutron irradiation has been observed in Fe9Cr-NiSiP_X1 and Fe9Cr-NiSiP_X2 alloys, despite the different dose rate. Thus, no significant temperature shift appears to be needed to compensate the dose rate for these alloys in the case of SRCs. In Fe9Cr_X0 (alloy with only 0.005 at% P), however, the number density and the P concentration of Cr-rich SRCs is lower after ion irradiation than under neutron irradiation. This reveals that some chemical compositions are more sensitive than others to dose-rate.
- The presence of Ni-Si-P appears to delay the onset of α' clusters formation in Fe9Cr alloys, for which the driving force for α' formation is low.
- Cr clustering is much less developed under ion irradiation and ballistic dissolution has been proposed as a reason for this.

6. Acknowledgements

This work was partially supported by the FP7 project MatISSE (Grant Agreement No. 604862), and by the Euratom research and training programme 2014-2018 M4F under grant agreement No. 755039. This work also contributes to the EERA (European Energy Research Alliance) Joint Programme on Nuclear Materials (JPNM). APT experiments were performed on the GENESIS platform. GENESIS is supported by the Région Haute-Normandie, the Métropole Rouen Normandie, the CNRS via LABEX EMC and the French National Research Agency as a part of the program “Investissements d’avenir” with the reference ANR-11-EQPX-0020. Parts of this research were carried out at the Ion Beam Center (IBC) at the Helmholtz-Zentrum Dresden - Rossendorf e. V., a member of the Helmholtz Association. We would like to thank Dr. C. Akhmadaliev for assistance.

[1] G.S. Was, J.T. Busby, T. Allen, E.A. Kenik, A. Jensson, S.M. Bruemmer, J. Gan, A.D. Edwards, P.M. Scott, P.L. Andreson, Emulation of neutron irradiation effects with protons: validation of principle, Journal of Nuclear Materials. 300 (2002) 198–216. https://doi.org/10.1016/S0022-3115(01)00751-6.

[2] A.D. Brailsford, R. Bullough, The rate theory of swelling due to void growth in irradiated metals, Journal of Nuclear Materials. 44 (1972) 121–135. https://doi.org/10.1016/0022-3115(72)90091-8.

[3] O. Tissot, C. Pareige, E. Meslin, B. Décamps, J. Henry, Influence of injected interstitials on α' precipitation in Fe–Cr alloys under self-ion irradiation, Materials Research Letters. 5 (2017) 117–123. https://doi.org/10.1080/21663831.2016.1230896.
[4] E.R. Reese, N. Almirall, T. Yamamoto, S. Tumey, G. Robert Odette, E.A. Marquis, Dose rate dependence of Cr precipitation in an ion-irradiated Fe18Cr alloy, Scripta Materialia. 146 (2018) 213–217. https://doi.org/10.1016/j.scriptamat.2017.11.040.
[5] G.S. Was, Emulating Neutron Irradiation Effects with Ions, in: G.S. WAS (Ed.), Fundamentals of Radiation Materials Science: Metals and Alloys, Springer, New York, NY, 2017: pp. 631–665. https://doi.org/10.1007/978-1-4939-3438-6_11.
[6] G.S. Was, T. Allen, Intercomparison of microchemical evolution under various types of particle irradiation, Journal of Nuclear Materials. 205 (1993) 332–338. https://doi.org/10.1016/0022-3115(93)90097-I.
[7] S.J. Zinkle, L.L. Snead, Opportunities and limitations for ion beams in radiation effects studies: Bridging critical gaps between charged particle and neutron irradiations, Scripta Materialia. 143 (2018) 154–160. https://doi.org/10.1016/j.scriptamat.2017.06.041.
[8] B. Heidrich, S.M. Pimblott, G.S. Was, S. Zinkle, Roadmap for the application of ion beam technologies to the challenges of nuclear energy technologies, Nuclear Instruments and Methods in Physics Research Section B: Beam Interactions with Materials and Atoms. 441 (2019) 41–45. https://doi.org/10.1016/j.nimb.2018.12.022.
[9] J.P. Wharry, G.S. Was, The mechanism of radiation-induced segregation in ferritic–martensitic alloys, Acta Mater. 65 (2014) 42–55. https://doi.org/10.1016/j.actamat.2013.09.049.
[10] J.L. Straalsund, The effect of cluster formation on the 'temperature shift' for accelerator simulation of neutron irradiation, Journal of Nuclear Materials. 51 (1974) 302–308. https://doi.org/10.1016/0022-3115(74)90195-0.
[11] R.M. Mayer, Nucleation and growth of voids by radiation: VII. Correlation of charged particle and neutron irradiations, Journal of Nuclear Materials. 95 (1980) 100–107. https://doi.org/10.1016/0022-3115(80)90085-9.
[12] N.H. Packan, K. Farrell, J.O. Stiegler, Correlation of neutron and heavy-ion damage: I. The influence of dose rate and injected helium on swelling in pure nickel, Journal of Nuclear Materials. 78 (1978) 143–155. https://doi.org/10.1016/0022-3115(78)90513-5.
[13] G.S. Was, Z. Jiao, E. Getto, K. Sun, A.M. Monterrosa, S.A. Maloy, O. Anderoglu, B.H. Sencer, M. Hackett, Emulation of reactor irradiation damage using ion beams, Scripta Materialia. 88 (2014) 33–36. https://doi.org/10.1016/j.scriptamat.2014.06.003.
[14] C. Pareige, V. Kuksenko, P. Pareige, Behaviour of P, Si, Ni impurities and Cr in self ion irradiated Fe–Cr alloys – Comparison to neutron irradiation, J. Nucl. Mater. 456 (2015) 471–476. https://doi.org/10.1016/j.jnucmat.2014.10.024.
[15] V. Kuksenko, C. Pareige, P. Pareige, Cr precipitation in neutron irradiated industrial purity Fe–Cr model alloys, J. Nucl. Mater. 432 (2013) 160–165. https://doi.org/10.1016/j.jnucmat.2012.07.021.
[16] M. Bachhav, G. Robert Odette, E.A. Marquis, α' precipitation in neutron-irradiated Fe–Cr alloys, Scripta Materialia. 74 (2014) 48–51. https://doi.org/10.1016/j.scriptamat.2013.10.001.
[17] F. Bergner, A. Ulbricht, C. Heintze, Estimation of the solubility limit of Cr in Fe at 300 °C from small-angle neutron scattering in neutron-irradiated Fe-Cr alloys, Scripta Mater. 61 (2009) 1060–1063. https://doi.org/10.1016/j.scriptamat.2009.08.028.
[18] Z. Jiao, G.S. Was, Segregation behavior in proton- and heavy-ion-irradiated ferritic–martensitic alloys, Acta Mater. 59 (2011) 4467–4481. https://doi.org/10.1016/j.actamat.2011.03.070.
[19] J.P. Wharry, Z. Jiao, V. Shankar, J.T. Busby, G.S. Was, Radiation-induced segregation and phase stability in ferritic–martensitic alloy T 91, J. Nucl. Mater. 417 (2011) 140–144. https://doi.org/10.1016/j.jnucmat.2010.12.052.
[20] F. Bergner, C. Pareige, M. Hernández-Mayoral, L. Malerba, C. Heintze, Application of a three-feature dispersed-barrier hardening model to neutron-irradiated Fe–Cr model alloys, Journal of Nuclear Materials. 448 (2014) 96–102. https://doi.org/10.1016/j.jnucmat.2014.01.024.

[21] V. Kuksenko, C. Pareige, C. Génevois, F. Cuvilly, M. Roussel, P. Pareige, Effect of neutron-irradiation on the microstructure of a Fe–12at.%Cr alloy, J. Nucl. Mater. 415 (2011) 61–66.
[22] M. Hernández-Mayoral, C. Heintze, E. Oñorbe, Transmission electron microscopy investigation of the microstructure of Fe–Cr alloys induced by neutron and ion irradiation at 300 °C, Journal of Nuclear Materials. 474 (2016) 88–98. https://doi.org/10.1016/j.jnucmat.2016.03.002.
[23] G. Monnet, Multiscale modeling of precipitation hardening: Application to the Fe–Cr alloys, Acta Materialia. 95 (2015) 302–311. https://doi.org/10.1016/j.actamat.2015.05.043.
[24] M.J. Konstantinović, L. Malerba, Mechanical properties of FeCr alloys after neutron irradiation, Journal of Nuclear Materials. (2019) 151879. https://doi.org/10.1016/j.jnucmat.2019.151879.
[25] A. Dubinko, N. Castin, D. Terentyev, G. Bonny, M.J. Konstantinović, Effect of Si–Ni–P on the emergence of dislocations loops in Fe–9Cr matrix under neutron irradiation: TEM study and OKMC modelling, Journal of Nuclear Materials. 540 (2020) 152395. https://doi.org/10.1016/j.jnucmat.2020.152395.
[26] N. Castin, G. Bonny, A. Bakaev, F. Bergner, C. Domain, J.M. Hyde, L. Messina, B. Radiguet, L. Malerba, The dominant mechanisms for the formation of solute-rich clusters in low-Cu steels under irradiation, Materials Today Energy. 17 (2020) 100472. https://doi.org/10.1016/j.mtener.2020.100472.
[27] M. Chiapetto, C.S. Becquart, L. Malerba, Simulation of nanostructural evolution under irradiation in Fe-9%CrC alloys: An object kinetic Monte Carlo study of the effect of temperature and dose-rate, Nuclear Materials and Energy. 9 (2016) 565–570. https://doi.org/10.1016/j.nme.2016.04.009.
[28] P.-M. Gueye, B. Gómez-Ferrer, C. Heintze, C. Pareige, Role of Ni, Si and P on the formation of solute-rich clusters under irradiation in Fe-Cr alloys, J. Nucl. Mater. (Submitted).
[29] C. Pareige, C. Heintze, M. Hernandez-Mayoral, F. Bergner, B. Gómez-Ferrer, E. Onobre, M. Konstantinovic, E. Meslin, O. Tissot, B. Décamps, P. Desgardin, R. Coppola, L. Malerba, MatISSE FP7-Fission-2013, D.2.3.1. Microstructural and mechanical characterisation of selected ion and neutron irradiated alloys, 2017.
[30] M. Matijasevic, A. Almazouzi, Effect of Cr on the mechanical properties and microstructure of Fe-Cr model alloys after n-irradiation, J. Nucl. Mater. 377 (2008) 147–154. https://doi.org/10.1016/j.jnucmat.2008.02.061.
[31] V. Kuksenko, Model Oriented Irradiation Experiments in Fe-Cr Model Alloys, PhD., University of Rouen, France, 2011.
[32] C. Heintze, F. Bergner, S. Akhmadaliev, E. Altstadt, Ion irradiation combined with nanoindentation as a screening test procedure for irradiation hardening, J. Nucl. Mater. 472 (2016) 196–205. http://dx.doi.org/10.1016/j.jnucmat.2015.07.023.
[33] J.F. Ziegler, J.P. Biersack, U. Littmark, The Stopping and Range of Ions in Solids, Pergamon, 1985. https://books.google.es/books?id=xclwQgAACAAJ.
[34] J.F. Ziegler, SRIM-2003, Nuclear Instruments and Methods in Physics Research Section B: Beam Interactions with Materials and Atoms. 219–220 (2004) 1027–1036. https://doi.org/10.1016/j.nimb.2004.01.208.
[35] ASTM E693, Standard Practice for Neutron Radiation Damage Simulation by Charged-Particle Irradiation, An- Nual Book of ASTM Standards, Vol. 12.02, American Society of Testing and Materials, West Conshohocken, PA. (1994) 12.02.
[36] R.E. Stoller, M.B. Toloczko, G.S. Was, A.G. Certain, S. Dwaraknath, F.A. Garner, On the use of SRIM for computing radiation damage exposure, Nucl. Inst. Meth. Phys. Res., Section B. 310 (2013) 75–80. https://doi.org/10.1016/j.nimb.2013.05.008.
[37] J.G. Gigax, E. Aydogan, T. Chen, D. Chen, L. Shao, Y. Wu, W.Y. Lo, Y. Yang, F.A. Garner, The influence of ion beam rastering on the swelling of self-ion irradiated pure iron at 450 °C, Journal of Nuclear Materials. 465 (2015) 343–348. https://doi.org/10.1016/j.jnucmat.2015.05.025.
[38] Lefebvre-Ulrikson, W, Vurpillot, F, Sauvage, X, Atom Probe Tomography - Put Theory into practice, San Diego : Elsevier Science, 2016.

[39] G. Da Costa, F. Vurpillot, A. Bostel, M. Bouet, B. Deconihout, Design of a delay-line position-sensitive detector with improved performance, Review of Scientific Instruments. 76 (2005) 013304–013304.
[40] C. Pareige, V. Kuksenko, P. Pareige, Behaviour of P, Si, Ni impurities and Cr in self ion irradiated Fe–Cr alloys – Comparison to neutron irradiation, J. Nucl. Mater. 456 (2015) 471–476. https://doi.org/10.1016/j.jnucmat.2014.10.024.
[41] J.M. Hyde, G. DaCosta, C. Hatzoglou, H. Weekes, B. Radiguet, P.D. Styman, F. Vurpillot, C. Pareige, A. Etienne, G. Bonny, N. Castin, L. Malerba, P. Pareige, Analysis of Radiation Damage in Light Water Reactors: Comparison of Cluster Analysis Methods for the Analysis of Atom Probe Data, Microscopy and Microanalysis. (2017) 1–10. https://doi.org/10.1017/S1431927616012678.
[42] B. Gómez-Ferrer, C. Heintze, C. Pareige, On the role of Ni, Si and P on the nanostructural evolution of FeCr alloys under irradiation, Journal of Nuclear Materials. (2019). https://doi.org/10.1016/j.jnucmat.2019.01.040.
[43] L. Messina, M. Nastar, T. Garnier, C. Domain, P. Olsson, Exact ab initio transport coefficients in bcc Fe-X (X=Cr,Cu,Mn,Ni,P,Si) dilute alloys, Phys. Rev. B. 90 (2014) 104203. https://doi.org/10.1103/PhysRevB.90.104203.
[44] L. Messina, T. Schuler, M. Nastar, M.-C. Marinica, P. Olsson, Solute diffusion by self-interstitial defects and radiation-induced segregation in ferritic Fe–X (X=Cr, Cu, Mn, Ni, P, Si) dilute alloys, Acta Materialia. 191 (2020) 166–185. https://doi.org/10.1016/j.actamat.2020.03.038.
[45] A. Hardouin-Duparc, Etude de la formation sous irradiation des amas de défauts ponctuels dans les alliages ferritiques faiblement alliés, PhD thesis, Paris XI-Orsay University, 1998.
[46] C. Domain, C.S. Becquart, Diffusion of phosphorus in α-Fe: An ab initio study, Phys. Rev. B. 71 (2005) 214109. https://doi.org/10.1103/PhysRevB.71.214109.
[47] E. Meslin, C.-C. Fu, A. Barbu, F. Gao, F. Willaime, Theoretical study of atomic transport via interstitials in dilute Fe − P alloys, Physical Review B. 75 (2007) 94303. https://doi.org/10.1103/PhysRevB.75.094303.
[48] F. Soisson, E. Meslin, O. Tissot, Atomistic modeling of α' precipitation in Fe-Cr alloys under charged particles and neutron irradiations: Effects of ballistic mixing and sink densities, Journal of Nuclear Materials. 508 (2018) 583–594. https://doi.org/10.1016/j.jnucmat.2018.06.015.